NASA Technical Memorandum 84479

Comparison of Viscous-Shock-Layer Solutions by Time-Asymptotic and Steady-State Methods

R. N. Gupta, J. N. Moss and A. L. Simmonds

May 1982

National Aeronautics and Space Administration

Langley Research Center
Hampton, Virginia 23665

COMPARISON OF VISCOUS-SHOCK-LAYER SOLUTIONS BY TIME-ASYMPTOTIC AND STEADY-STATE METHODS

By

R. N. Gupta*, J. N. Moss, and A. L. Simmonds
Langley Research Center

SUMMARY

An evaluation has been made of two flow-field codes employing the time- and space-marching numerical techniques. The space-marching technique considered is an implicit finite-difference method due to Davis. The time-marching method employs the time-asymptotic, two-step, finite-difference method of MacCormack. These two methods have been used to analyze the flow field around a massively blown Jupiter entry probe under perfect-gas conditions. In order to obtain a direct point-by-point comparison, the computations by the two schemes have been done by using identical grids and turbulence models. For the same degree of accuracy, the space-marching scheme takes much less time as compared to the time-marching method and would appear to provide accurate results for the problems with nonequilibrium chemistry, free from the effect of local differences in time on the final solution which is inherent in time-marching methods. With the time-marching method, however, the solutions are obtainable for the realistic entry probe shapes with massive or uniform surface blowing rates, whereas with the space-marching technique, it is difficult to obtain converged solutions for such flow conditions. The choice of the numerical method is, therefore, problem dependent. Both the methods give equally good results for the cases where a comparison with the experimental data has been made.

---

*NRC-Senior Research Associate.

INTRODUCTION

Recently an evaluation[1] of the three different flow-field codes[2,3,4] was presented. These codes were primarily developed for the hypersonic, massively blown, and strongly radiating shock layers with application to the Jupiter entry conditions. Evaluation and comparison of the codes are important because of the dependence of the Galileo heat-shield design on these flow-field solutions. However, direct comparisons have been hampered by the fact that the three codes use different solution procedures, different computational mesh sizes, different chemical and turbulence models, different convergence criteria, as well as a different number of computational nodes along and perpendicular to the body. Even for the only common feature of radiative transport code, there are subtle differences in the spectral details of some species. Thus, for an objective evaluation of the different numerical solution methods employed by these codes, it would be desirable to select a simple no-blowing perfect-gas flow-field case for which the turbulent models are well established. The purpose of this paper is to present the results of such a study. The results have been obtained by employing two of the three numerical codes mentioned earlier. The first[2] of these two is a space-marching method that solves the steady-state viscous-shock-layer type equations by the method of Davis.[5] The second one[3] is a time-marching method that employs the time-asymptotic, two-step, finite-difference method of MacCormack[6] for the solution of time-dependent viscous-shock-layer type equations. The third numerical code[4] uses an inverse analytical method. Since the method of reference 4 also falls under the category of a space-marching method (similar to the category of method of ref. 2), it has not been included in the present comparison. The work presented here includes the

results for a blown perfect-gas viscous shock layer by the space- and time-marching numerical methods. The comparative study of these two methods shows their relative merits and disadvantages for a blown and unblown shock layer. The present results may also be helpful in resolving the differences[1] in predicted results by the different codes for the Jupiter entry conditions.

ANALYSIS

As mentioned earlier, the space-marching (perfect-gas version of HYVIS[2]) and the time-marching codes (perfect-gas version of COLTS[3]) have been employed to predict the perfect-gas forebody flow field for Jupiter entry-type conditions. For this study, these two codes employ the same grid spacing along and perpendicular to the body, and the same number of computational mesh nodes in the streamwise and normal directions. The flow for both of these methods undergoes transition instantaneously to turbulent flow at the first body station downstream of the stagnation point. The two methods also employ the same turbulence model[7,8] with and without blowing. For the case which includes blowing, identical blowing-rate distribution as shown in figure 1 has been used.

The governing equations employed in the present study can be obtained from the unsteady/steady Navier-Stokes equations by keeping terms up to second order in the inverse square root of the Reynolds number in both the viscous and inviscid regions. These equations, when modified for turbulent flow by using methods analogous to those presented by Dorrance,[9] provide perfect-gas governing equations for the space-[8] and time-marching[10] methods.

In addition to the surface blowing rate distribution of figure 1, the boundary conditions employed along the body surface are no velocity slip and temperature jump. The wall temperature is taken as a constant specified

value. For the time-marching method, the wall pressure is taken equal to the pressure at the adjacent grid point in the normal direction. The conditions imposed at the shock are calculated by using the Rankine-Hugoniot shock relations. These relations in the body-oriented coordinates (for use with the time-marching method) are provided in reference 11. The flow conditions along the supersonic outflow boundary are determined by extrapolation from the inner mesh points for the time-marching scheme. No such flow conditions are required for the space-marching method. Further, for the present study, Sutherland's equation

$$\mu^* = \mu^*_\infty \left(\frac{T^*}{T^*_\infty}\right) \left(\frac{1 + \frac{C^*}{T^*_\infty}}{1 + \frac{C^*}{T^*}}\right) \tag{1}$$

has been used to determine the viscosity, and the coefficient of thermal conductivity is computed by assuming a constant Prandtl number:

$$k^* = \frac{\gamma R^* \mu^*}{(\gamma - 1)Pr} \tag{2}$$

In equations (1) and (2), the quantities with an asterisk are dimensional and R^* is the gas constant.

In order to obtain a direct point-by-point comparison and to keep the same truncation error in the finite-difference approximations employed in the space- and time-marching schemes, the computations by the two schemes have been done by using identical grids. The following logarithmic grid-spacing

$$\bar{n} = \frac{\ell n \left[\frac{\beta + (1 - \frac{n}{\delta})}{\beta - (1 - \frac{n}{\delta})}\right]}{\ell n \left[\frac{\beta + 1}{\beta - 1}\right]} \tag{3}$$

has been used in the two methods in the direction normal to the body to allow higher resolution near the body surface. In equation (3), β is the grid-stretching factor, $n(=n^*/r_N^*)$ is the normal coordinate, and $\delta(=\delta^*/r_N^*)$ is the shock standoff distance. Finally, the following convergency criterion has been employed for both blown as well as unblown cases:

$$\underset{i,j}{\text{maximum}} \left| \frac{\left(\frac{\partial H}{\partial n}\right)^k - \left(\frac{\partial H}{\partial n}\right)^{k-500}}{\left(\frac{\partial H}{\partial n}\right)^k_{i=1}} \right| < \varepsilon \qquad (4a)$$

where ε is of order 10^{-2}. In equation (4a), $H(=H^*/u_\infty^{*2})$ is the nondimensional total enthalpy; i is the finite-difference point in the direction along the body surface (or s-direction); j is the finite-difference point normal to the body surface (or n-direction); and k is the kth time step. For the space-marching method, convergence criterion of relation (4a) is modified to:

$$\underset{i,j}{\text{maximum}} \left| \frac{\left(\frac{\partial H}{\partial n}\right)^\ell - \left(\frac{\partial H}{\partial n}\right)^{\ell-1}}{\left(\frac{\partial H}{\partial n}\right)^\ell_{i=1}} \right| < \varepsilon \qquad (4b)$$

where ℓ is the global iteration count.

As indicated in the Introduction, the present comparative study of the space-[5] (due to Davis) and time-[6] (due to MacCormack) marching methods has been done by employing these methods as described in references 2 and 3, respectively. Since the present methods of solution are identical to those of references 2 and 3, these are not presented here. Briefly, since the time-marching algorithm[6] is explicit and amenable to complete vectorization, it has been programed on a vector processor (CYBER 203). The solutions with

the space-marching implicit-difference scheme[5] have been obtained on CYBER 175. Further, in order to speed up the calculations with the time-marching method, the largest possible Courant-Friedrichs-Lewy (CFL) time-step size for each mesh point has been used in preference to the global minimum CFL time-step size.

DISCUSSION OF RESULTS

First, a comparison of the predictions made by the space- and time-marching methods against the available experimental data is given. There are no experimental data available, for the turbulent viscous-shock-layer problem (at high Reynolds number) with massive surface blowing considered here. For the laminar viscous-shock-layer flow at moderate Reynolds number, a comparison between the predictions made by the two methods and the experimental data is contained in figure 12 of reference 12. Both the methods predict the heating rate for a 45° half-angle cone which compares favorably with the experimental data. For the low Reynolds number case, the predictions by the space- and time-marching methods are compared against the experimental data of reference 13 in figure 2 for a 45° half-angle hyperboloid. Once again, the comparison between the predictions by the two methods and the experimental data is quite good at $Re_{\infty}=90$. At $Re_{\infty}=1035$, the predictions depart from the experimental data. However, the two predictions compare favorably with each other.

Next, flow-field results and surface heating rates obtained by the space- and time-marching methods are presented for the forebody of a 44.25° half-angle sphere-cone probe entering the Orton nominal (0.895 H_2 + 0.105 He)

Jupiter atmosphere under perfect-gas assumption. Results have been obtained with and without surface blowing assuming instantaneous transition at the first grid point downstream of the stagnation point. The freestream conditions and other parameters employed in the analysis have been taken from the peak heating entry conditions at 51.5 seconds for the 310-kg probe.[14] These are given below:

Nose radius, $r_N^* = 0.352$ m

Free stream Mach number, $M_\infty = 43.76$

Free stream temperature, $T_\infty^* = 151.2$ K

Free stream density, $\rho_\infty^* = 4{,}966 \times 10^{-4}$ kg/m^3

Probe surface temperature, $T_w^* = 4022.80$ K

Ratio of specific heats, $\gamma = 1.4$

Gas constant, $R^* = 3737.45$ J/kg K

Reynolds number, $Re = \dfrac{r_N^* u_\infty^* \rho_\infty^*}{\mu_\infty^*} = 1.2274 \times 10^6$

Prandtl number, $Pr = 0.72$

Mixture molecular weight, $\bar{m} = 2.2246$

Computations by both space- and time-marching methods employed a constant step size $\Delta s(\Delta s^*/r_N^*) = 0.1597$ in the direction along the body surface and a total of 15 body stations were used. In the direction perpendicular to the body, the grid was generated as given by equation (3) and altogether 101 points

were used with a constant step size $\Delta n = 0.01$. Depending on the value of β in equation (3), this step size gives a finer resolution near the body surface in the physical s^*, n^* - plane. Two values of β (1.1 and 1.01) were employed in the computations. For the first value of β, the first grid point off the body surface is located at 0.295 percent of the shock standoff distance as compared with 0.05418 percent for $\beta = 1.01$. The various results computed by the two methods are displayed in figures 3 through 9 and are discussed in the following paragraphs.

Figures 3(a) and 3(b) contain the surface pressure distributions and the shock standoff distances obtained from the two methods with and without surface blowing conditions. Except for the region near the tangency point, both these methods give comparable results. The results obtained by the two codes at the juncture point should not be taken seriously due to the curvature discontinuity there. For an unblown shock layer, the method of characteristics does give[15] a fast pressure recovery at the tangency point similar to the one obtained by the space-marching method. The fourth-order damping employed with the time-marching method smears out the effect of surface discontinuity, since a large number of global iterations is used to obtain a converged solution.

Figures 4 through 7 show velocity and temperature distributions over both the spherical ($s = 0.64$) and the conical flank ($s = 1.76$) portions of the probe. There is reasonable agreement between the various results obtained by the two computational methods. However, if the results near the wall (figs. 5 and 7) are analyzed carefully, the slopes of the velocity and temperature profiles for $\beta = 1.1$ and no surface blowing ($m_o = 0$) are

seen to be quite different. With the reduction in the value of β to 1.01, the slopes predicted by the two methods begin to agree quite well. Reducing β further does not result in any noticeable improvement. The surface pressure distribution, shock standoff distance, and gross features of the velocity and temperature profiles are unaffected by reducing β from 1.1 to 1.01. As will be seen later, the quantities affected most by the mesh refinement near the surface are the wall heat transfer and skin friction, as expected. Figures 5 and 7 also indicate that with the coarser normal-direction mesh (β = 1.1), results obtained by the space-marching method are closer to the finer mesh (β = 1.01) results. With surface blowing, the mesh refinement near the surface does not affect the slopes there substantially. A mesh refinement obtained with β = 1.1 appears adequate. Use of the largest possible value of β without jeopardizing the accuracy of the results is important, since the computational time is reduced by almost 20 percent for the time-dependent method when β is increased from 1.01 to 1.1 for the same convergence criterion of equation (4a). Yet if a large value of β is used with small surface blowing rates, then poor resolution of the maximum gradients may occur.

The eddy viscosity distributions over the spherical and conical portions of the probe are given in figs. 8(a) and 8(b). There is reasonable agreement with respect to the maximum values and the general character of the distributions obtained by the two methods. It may be mentioned again that the identical turbulence models[7,8] have been used with the two computational methods.

Finally, figs. 9(a) through 9(c) give the skin-friction, dimensional and nondimensional (Stanton number) heating rates at the wall. As indicated earlier, there is better agreement between the results obtained with a fine mesh ($\beta = 1.01$) for the unblown case. For the blown surface case, the two numerical methods give good results for even the coarse mesh ($\beta = 1.1$). Generally, the results are in better agreement over the conical flank portion than over the spherical portion or near the juncture point.

Computationally, in absence of blowing, the space-marching method is quite economical and gives results which compare well with the experimental data. However, with large blowing and arbitrary body shapes, the time-marching method has proved to provide solutions without the numerical instability experienced with the space-marching method. Without blowing and for analytic body shapes, both methods appear equally accurate.

Further, the time-marching method has been used to predict flows with large embedded subsonic regions.[16] Some recent efforts[17] have also been made to handle such flows with the space-marching method by making use of certain approximations to improve the initial marching profiles. The advantage of the space-marching method in such cases lies in the fact that for problems requiring more computational grid points (either due to the large body size or large Reynolds number of the flow) the storage and computational time requirements are much less as compared to the time-marching method. Also, with the time-marching method, the computational time increases substantially if more grid points are clustered in the shear layer, whereas with the space-marching method, the computational time is not significantly affected by distribution of the grid points in the shear layer. The computational time of the time-marching method, however, can be reduced substantially by employing its recent implicit analogue.[18]

Finally, for a viscous reacting flow with nonequilibrium chemistry, there are three time-step criteria[19] used with the time-marching method, namely: the Courant-Friedrichs-Lewy (CFL) criterion, a viscous dissipation criterion, and a species production criterion. Therefore, the solution of the species equation proceeds with a time step which is different from the one used with the momentum and energy equations. For the nonequilibrium chemistry calculations, such local differences in time will affect the final relaxed solution, since in going through the transient part of the solutions one would produce or deplete species at a rate which may not be characteristic of the final converged solutions. Unlike the case with equilibrium chemistry, the nonequilibrium chemistry cannot correct itself as the velocity and temperature fields converge to the steady state values. The space-marching method,[20] however, appears to be free from this drawback.

Thus, the choice of the numerical method is rather problem dependent. Both methods give comparable results for the problems where comparisons with the experimental data have been made, provided that care is taken in selecting the appropriate mesh size near the body surface.

CONCLUDING REMARKS

The space-marching implicit technique of Davis and the time-marching explicit method of MacCormack have been used to analyze the flow field around a massively blown Jupiter entry probe under perfect gas conditions. These two techniques have been widely used for the heat shield design calculations for such a probe. Certain differences are known to exist in the predicted results by the two techniques. In order to isolate these differences, a point by point comparison of the various flow-field quantities computed by the two schemes has been obtained by using identical computational grids and turbulence models. Generally, the results obtained by the two methods are in better

agreement over the conical flank portion than over the spherical portion or near the juncture point. For the same degree of accuracy, the space-marching scheme takes much less time and would appear to provide accurate results for the problems with nonequilibrium chemistry, free from the effect of local differences in time on the final solution which are inherent in time-marching methods. With the time-marching method, however, the solutions are obtained for the realistic entry-probe shapes with massive blowing rates, whereas with the space-marching technique, it is difficult to obtain converged solutions for such flow conditions. The choice of the numerical method is, therefore, problem dependent. Both the methods give comparable results for the problems where comparisons with the experimental data have been made, provided that care is taken in selecting the appropriate mesh size near the body surface.

REFERENCES

1. Menees, G. P.: An Evaluation of Computer Codes for Simulating the Galileo Probe Aerothermal Entry Environment. AIAA Paper 81-1069, June 1981.

2. Moss, J. N.: A Study of the Aerothermal Entry Environment for the Galileo Probe. AIAA Paper 79-1081, June 1979.

3. Kumar, A.; Graves, R. A., Jr.; Weilmuenster, K. J.; and Tiwari, S. N.: Laminar and Turbulent Flow Solutions with Radiation and Ablation Injection for Jovian Entry. AIAA Paper 80-0288, January 1980.

4. Nicolet, W. E. and Balakrishnan, A.: Methods for Predicting Off-Stagnation Point Flow Fields for Planetary Entry Probes. AIAA Paper 79-1083, June 1979.

5. Davis, R. T.: Numerical Solution of the Hypersonic Viscous-Shock-Layer Equations. AIAA Journal, vol. 8, no. 5, May 1970, pp. 843-851.

6. MacCormack, R. W.: The Effect of Viscosity in Hypervelocity Impact Cratering. AIAA Paper 69-354, April 1969.

7. Cebeci, T.: Behavior of Turbulent Flow Near a Porous Wall with Pressure Gradient. AIAA Journal, vol. 8, no. 12, December 1970, pp. 2152-2156.

8. Anderson, E. C. and Moss, J. N.: Numerical Solution of the Hypersonic Viscous-Shock-Layer Equations for Laminar, Transitional, and Turbulent Flows of a Perfect Gas Over Blunt Axially Symmetric Bodies. NASA TN D-7865, February 1975.

9. Dorrance, W. H.: Viscous Hypersonic Flow. McGraw-Hill Book Company, Inc., 1962.

10. Kumar, A.; Graves, R. A., Jr. and Tiwari, S. N.: Laminar and Turbulent Flows Over a Spherically Blunted Cone with Massive Surface Blowing. AIAA Journal, vol. 17, no. 12, December 1979, pp. 1326-1331.

11. Xerikos, J. and Anderson, W. A.: A Time-Dependent Approach to the Numerical Solution of the Flow Field About a Axisymmetric Vehicle at Angle of Attack. NASA CR-61982, 1968.

12. Kumar, A. and Graves, R. A., Jr.: Numerical Solution of the Viscous Hypersonic Flow Past Blunted Cones at Angle of Attack. AIAA Paper 77-172, January 1977.

13. Little, H. R.: An Experimental Investigation of Surface Conditions on Hyperboloids and Paraboloids at a Mach Number of 10. M.S. Thesis, University of Tennessee, 1969.

14. Moss, J. N. and Kumar, A.: Significance of Turbulence and Transition Location on Radiative Heating With Ablation Injection. AIAA Paper 81-0281, January 1981.

15. Anderson, E. C.; Moss, J. N. and Sutton, K.: Turbulent Viscous-Shock-Layer Solutions With Strong Vorticity Interaction. AIAA Paper 76-120, January 1976.

16. Rizk, Y. M.; Chaussee, D. S. and McRay, D. S.: Computation of Hypersonic Viscous Flow Around Three-Dimensional Bodies at High Angles of Attack. AIAA Paper 81-1261, June 1981.

17. Thareja, R.; Szema, K. Y. and Lewis, C. H.: Viscous Shock-Layer Predictions for Hypersonic Laminar or Turbulent Flows in Chemical Equilibrium Over the Windward Surface of a Shuttle-Like Vehicle. AIAA Paper 82-0201, January 1982.

18. MacCormack, R. W.: A Numerical Method for Solving the Equations of Compressible Viscous Flow. AIAA Paper 81-0110, January 1981.

19. Li, C. P. : Hypersonic Nonequilibrium Flow Past a Sphere at Low Reynolds Numbers. AIAA Paper 74-173, 1974.

20. Moss, J. N.: Reaching Viscous-Shock-Layer Solutions With Multicomponent Diffusion and Mass Injection. NASA TR R-411, June 1974.

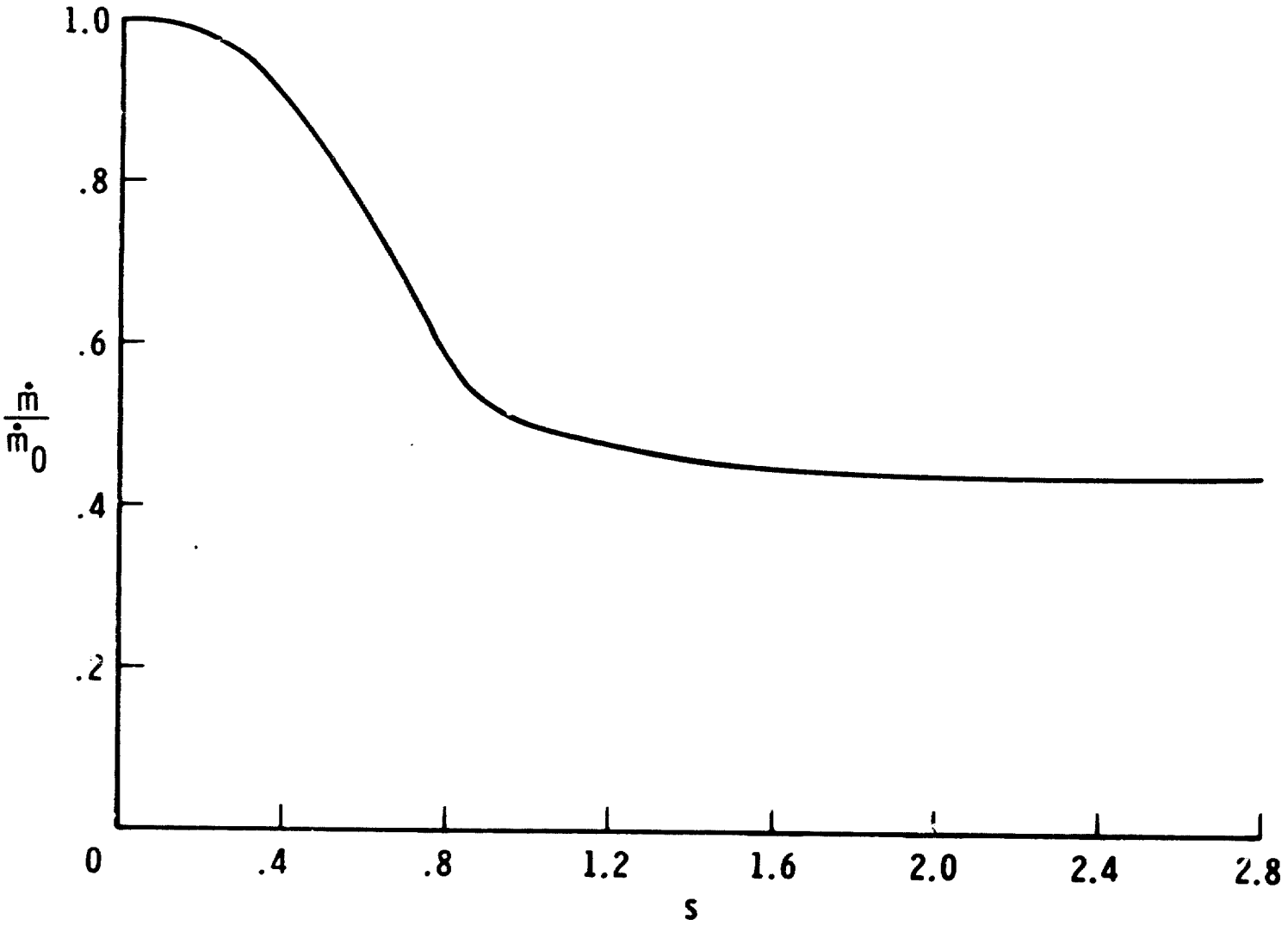

Fig. 1 Nondimensional blowing rate distributions along the surface.

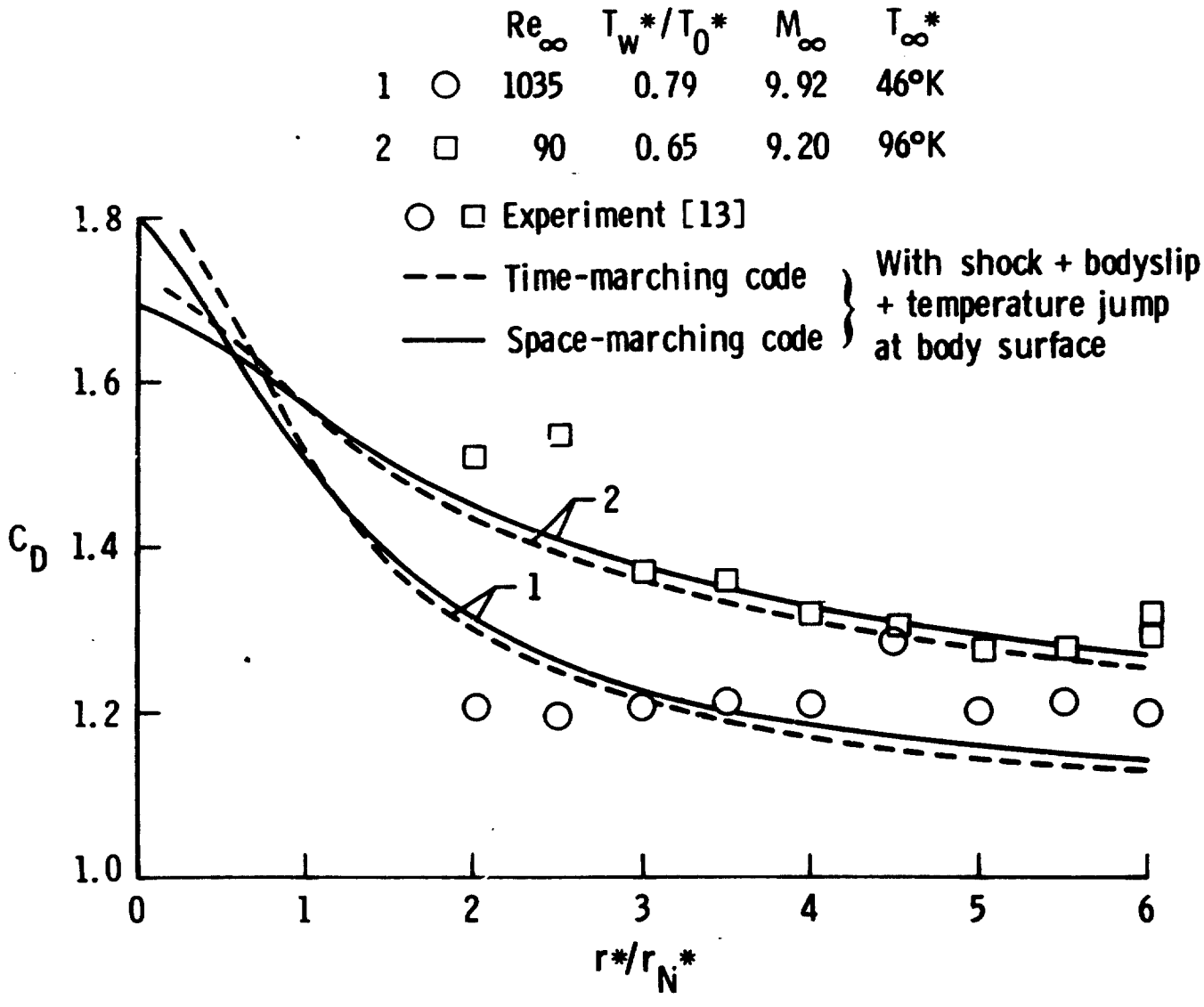

Fig. 2 Total drag coefficient for a 45^0 half-angle hyperboloid.

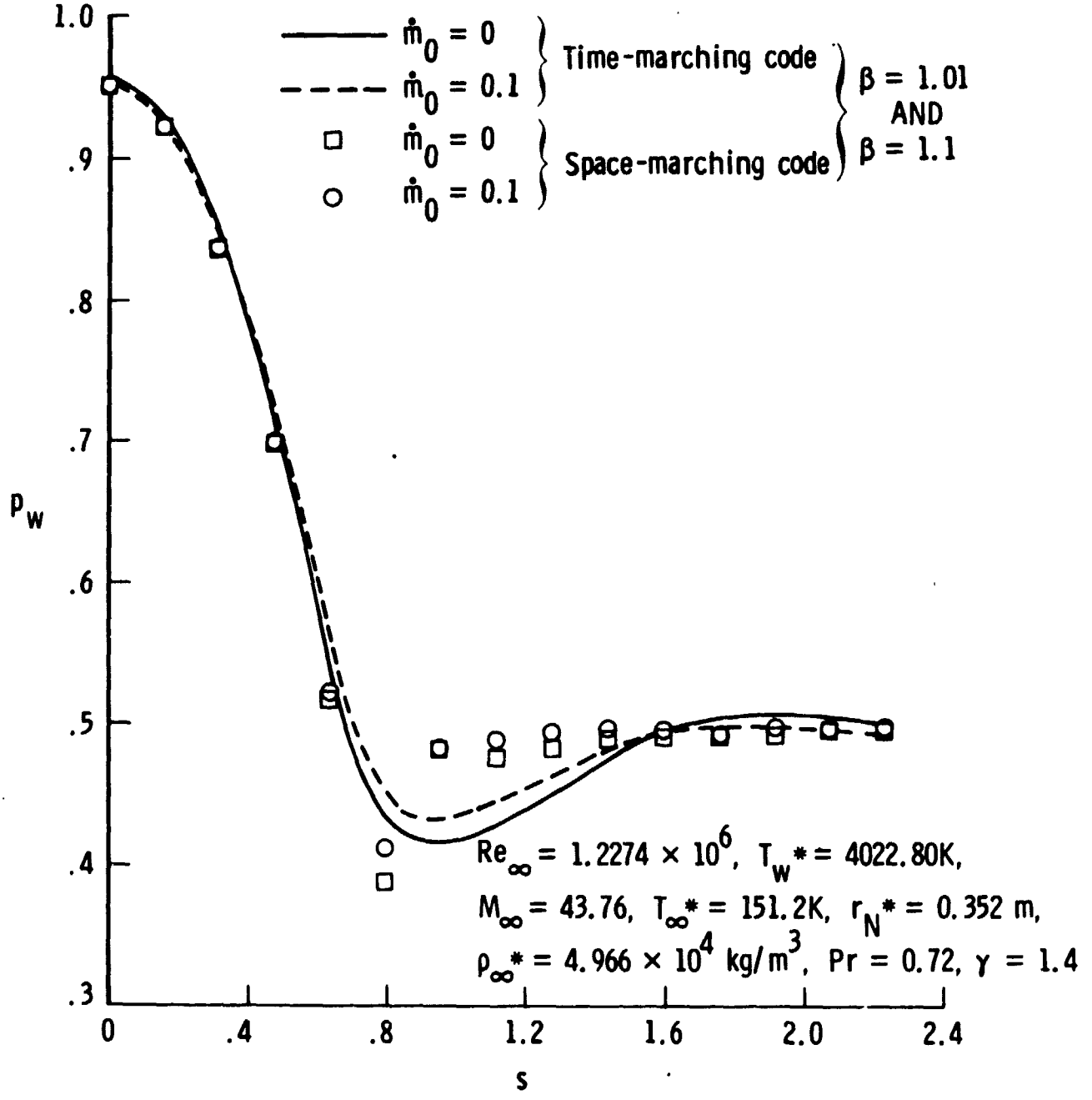

(a) Surface pressure distribution.

Fig. 3 Comparison of time-marching and space-marching solutions both with and without blowing.

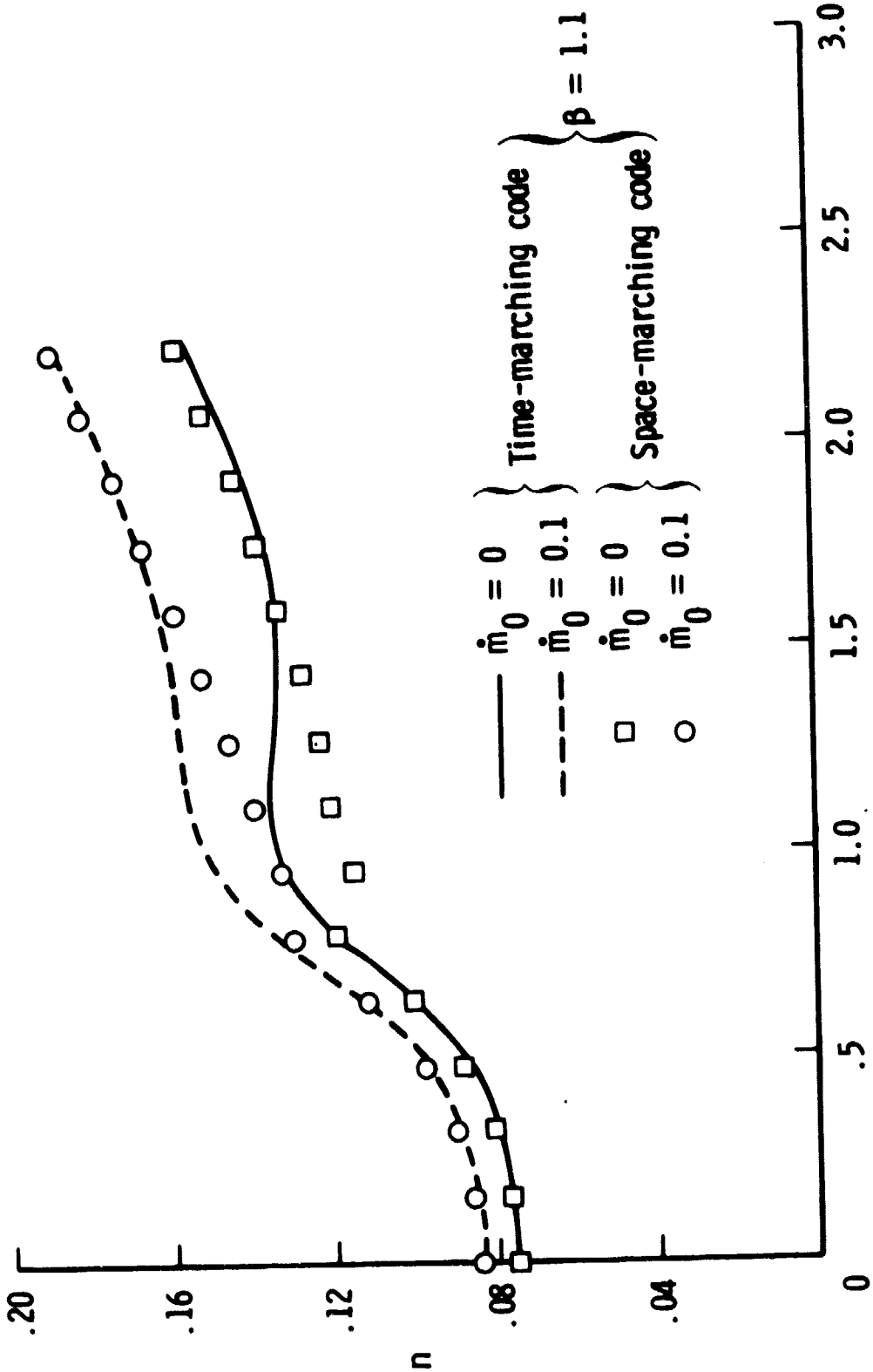

(b) Shock standoff distribution.

Fig. 3 Concluded.

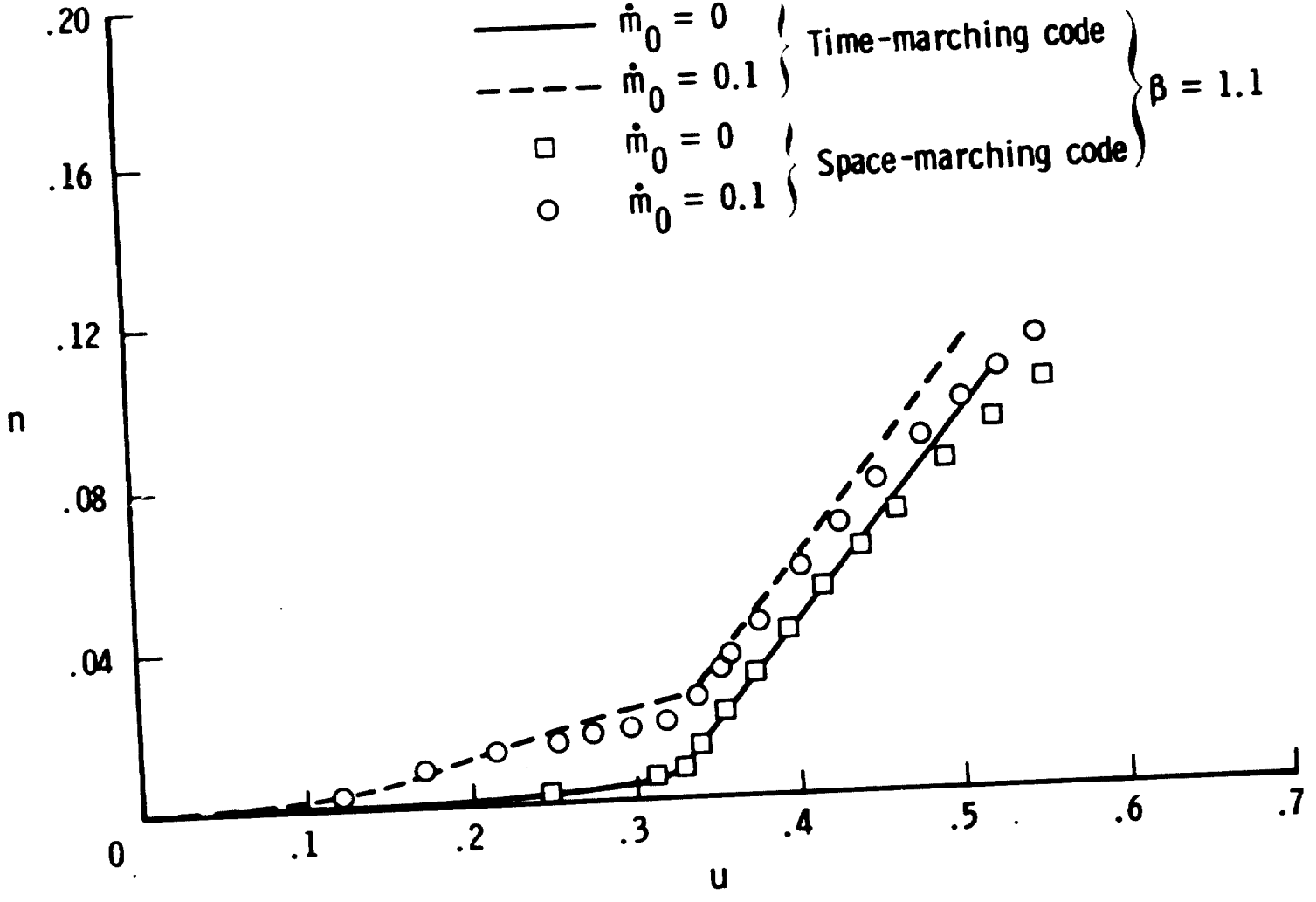

(a) s = 0.64.

Fig. 4 Comparison of tangential velocity profile predictions.

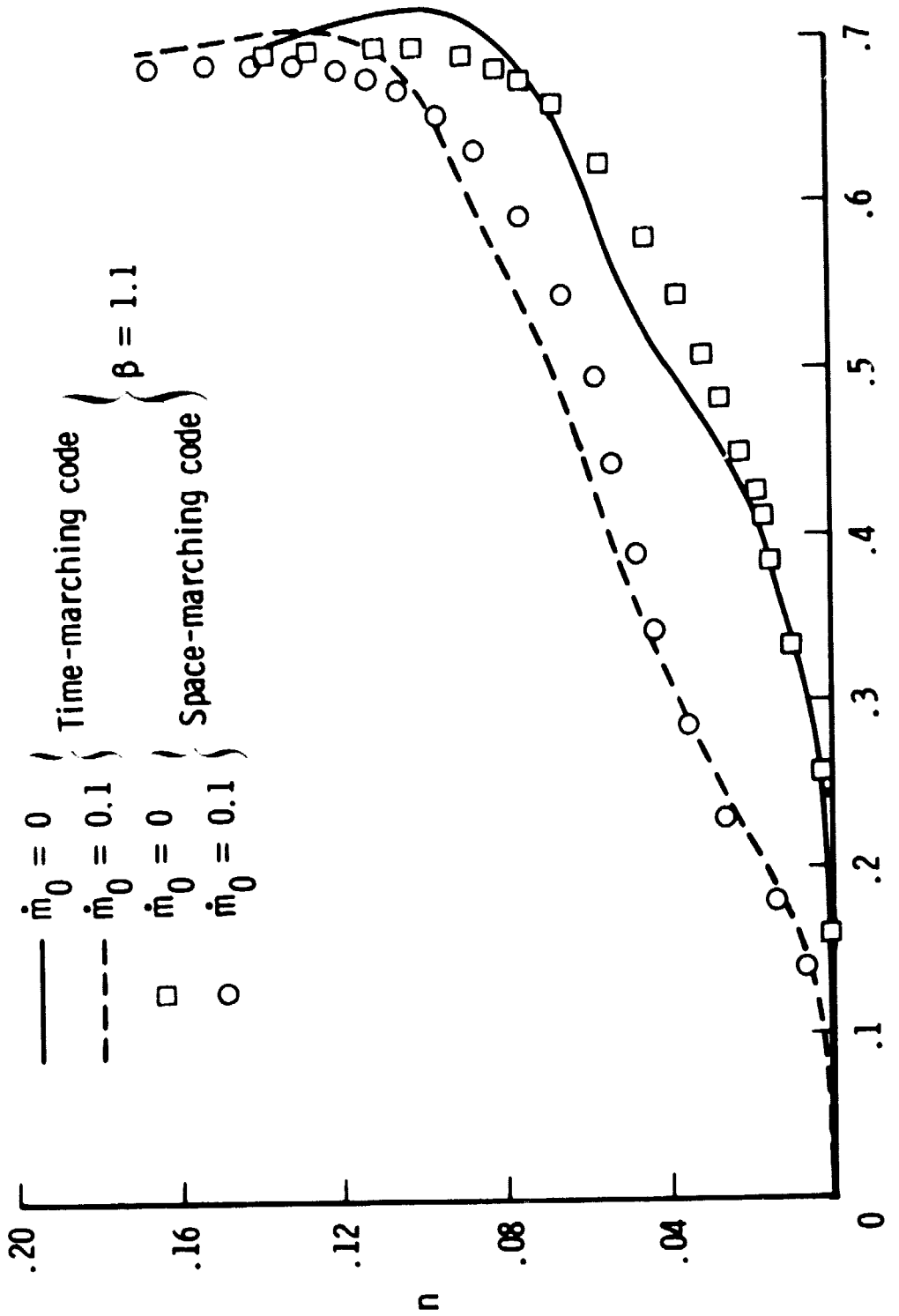

(b) s = 1.76.

Fig. 4 Concluded.

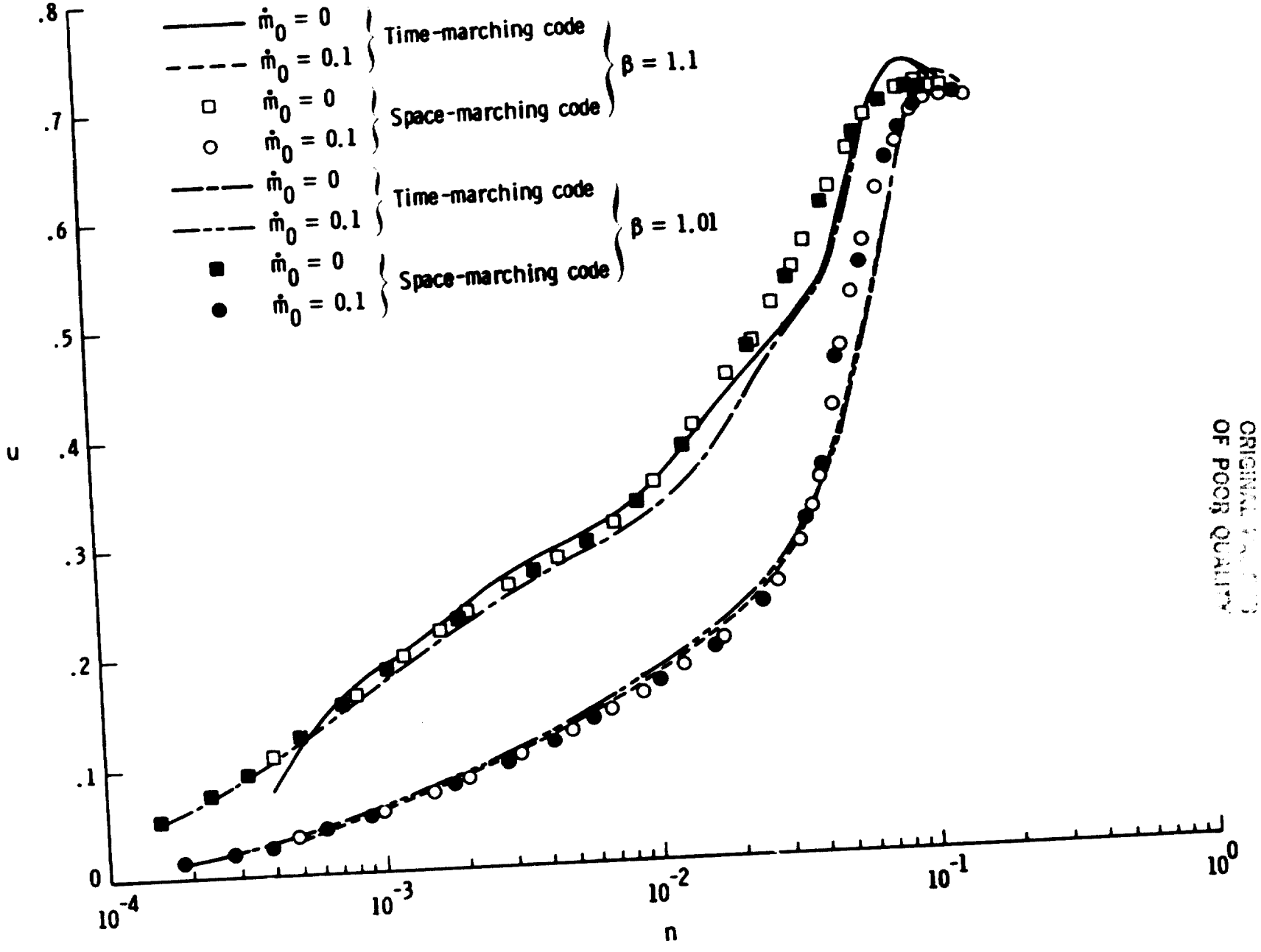

Fig. 5 Effect of normal grid spacing on predicted tangential velocity profiles (s = 1.76).

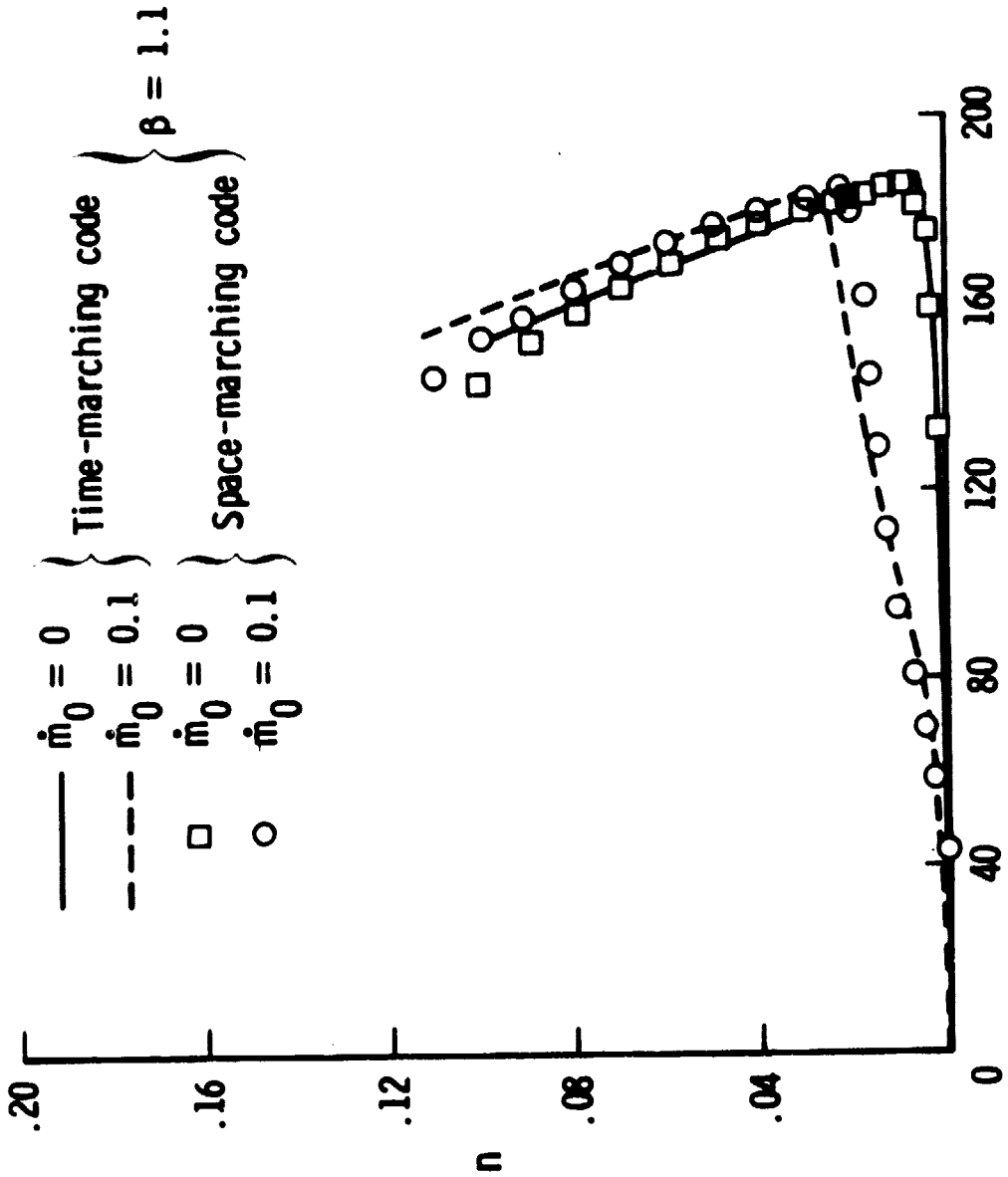

(a) s = 0.64.

Fig. 6 Comparison of temperature profile predictions.

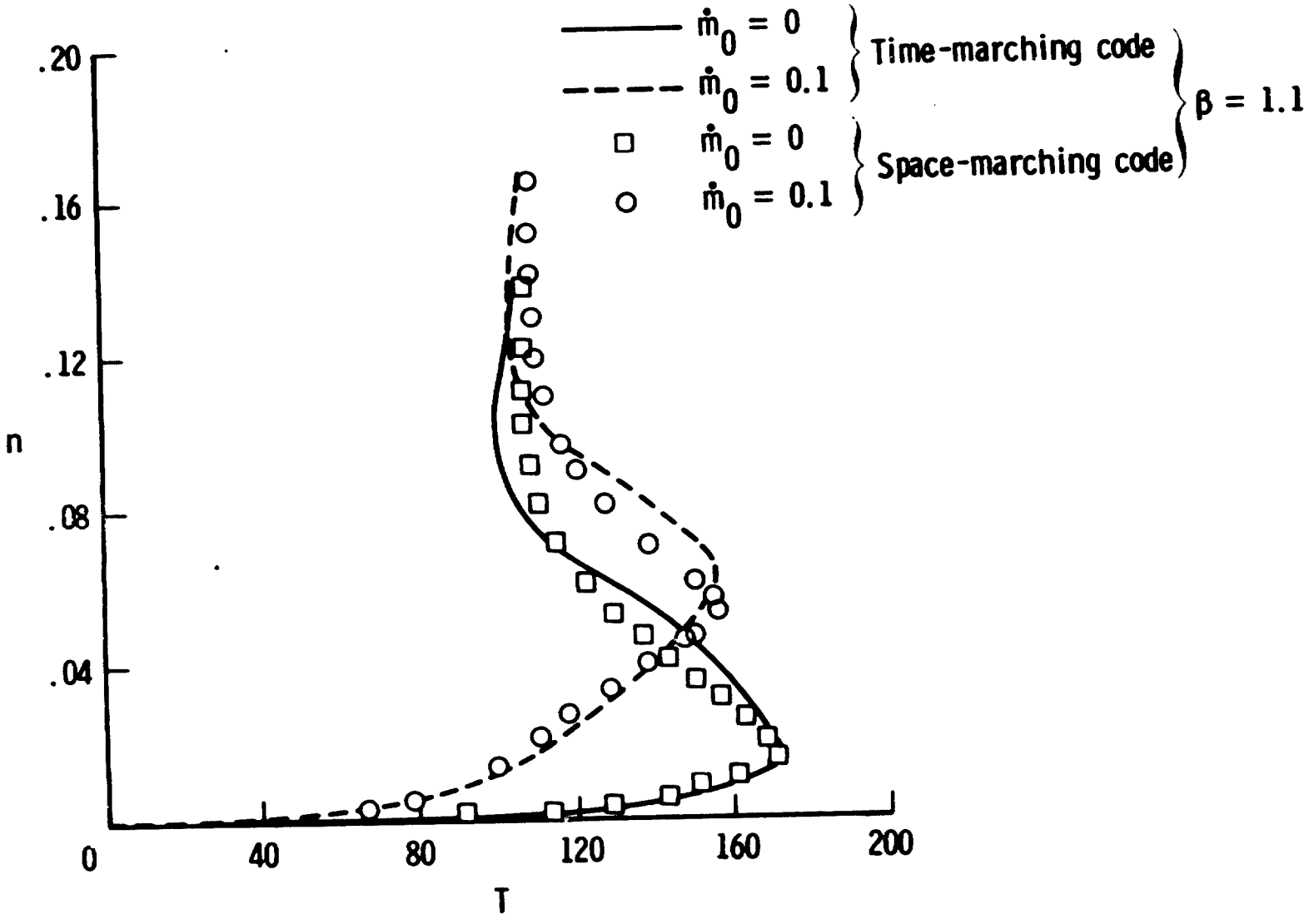

(b) s = 1.76.

Fig. 6 Concluded.

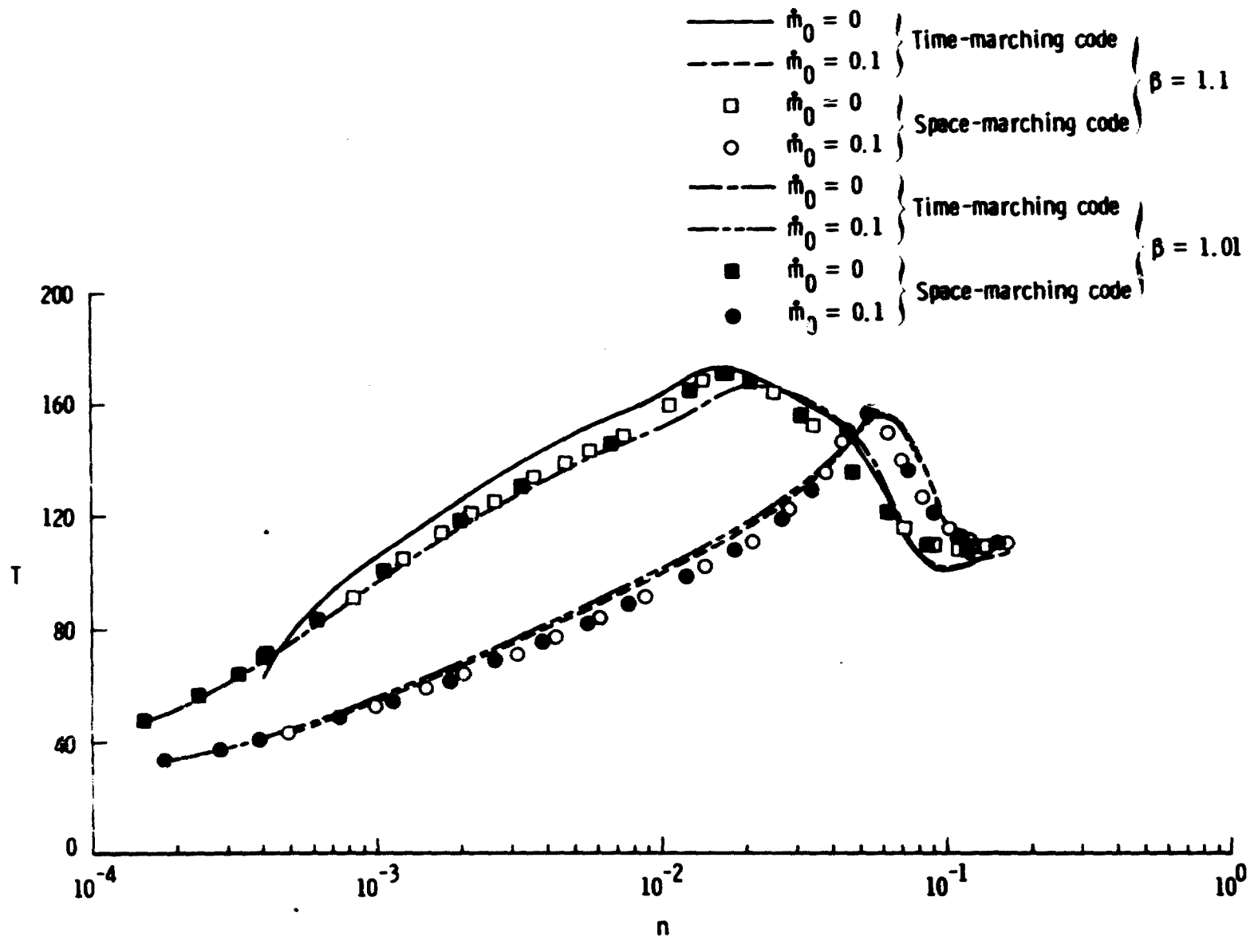

Fig. 7 Effect of normal grid spacing on predicted temperature profiles.

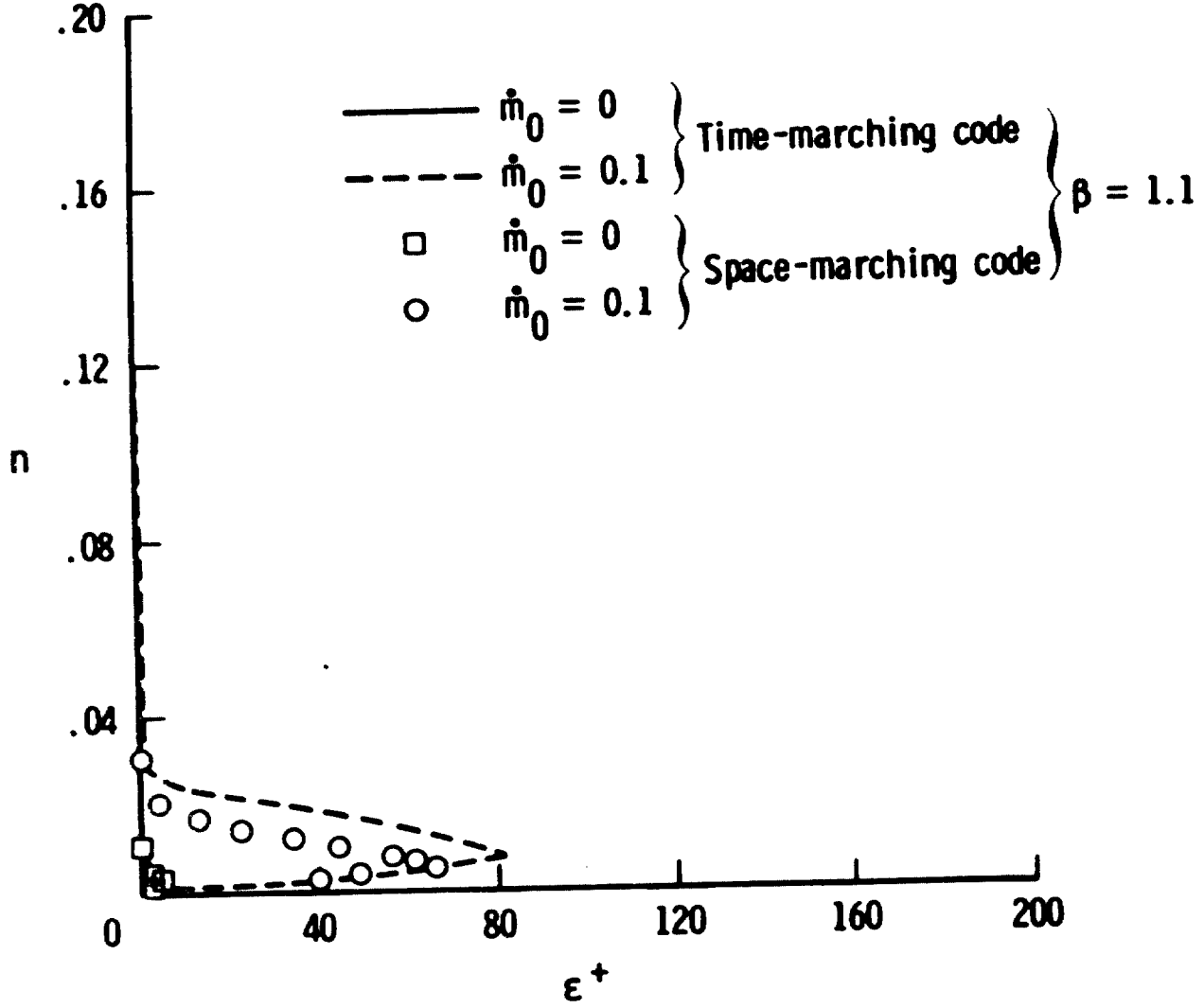

(a) s = 0.64.

Fig. 8 Comparison of predicted eddy viscosity profiles.

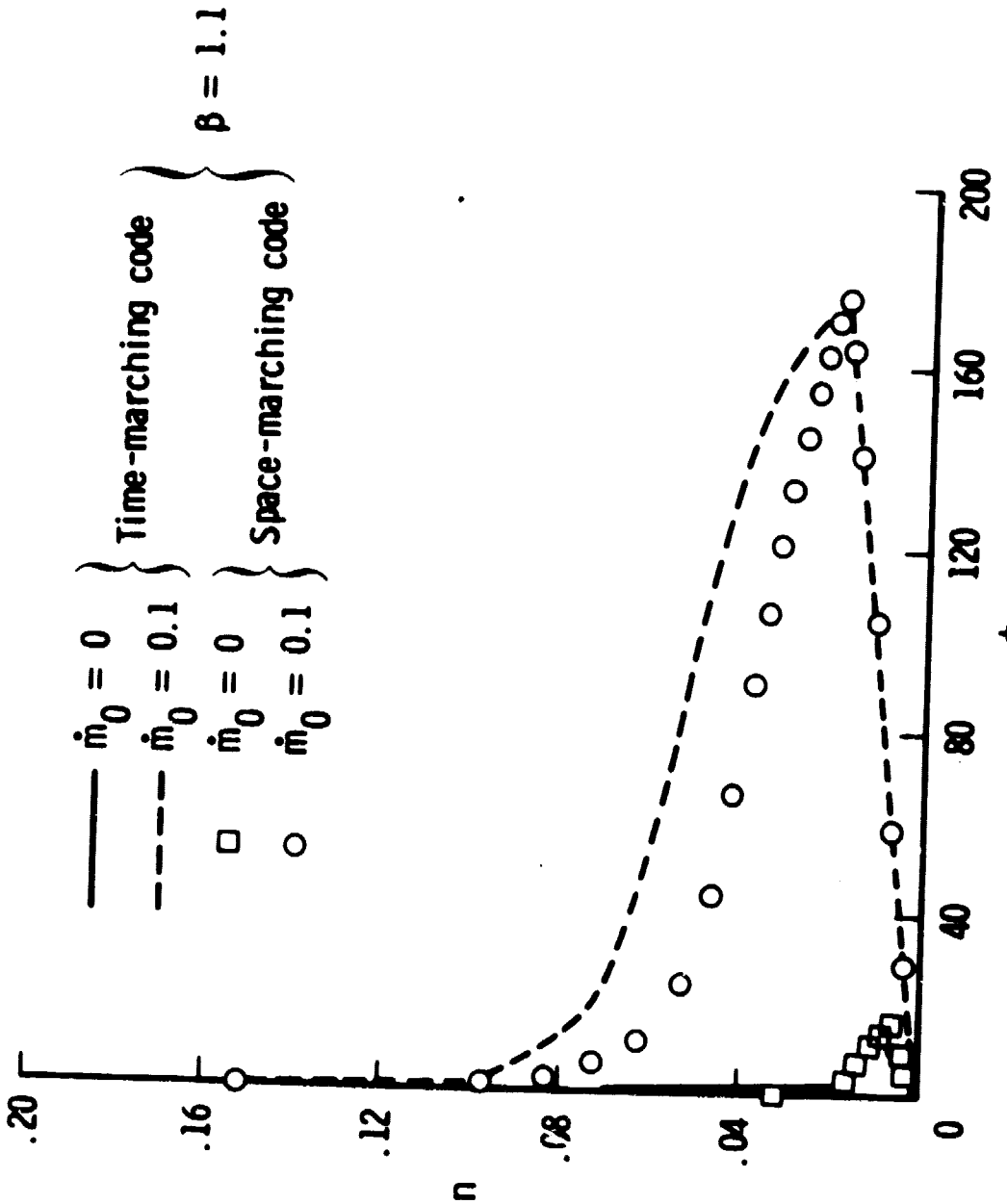

(b) $s = 1.76$.

Fig. 8 Concluded.

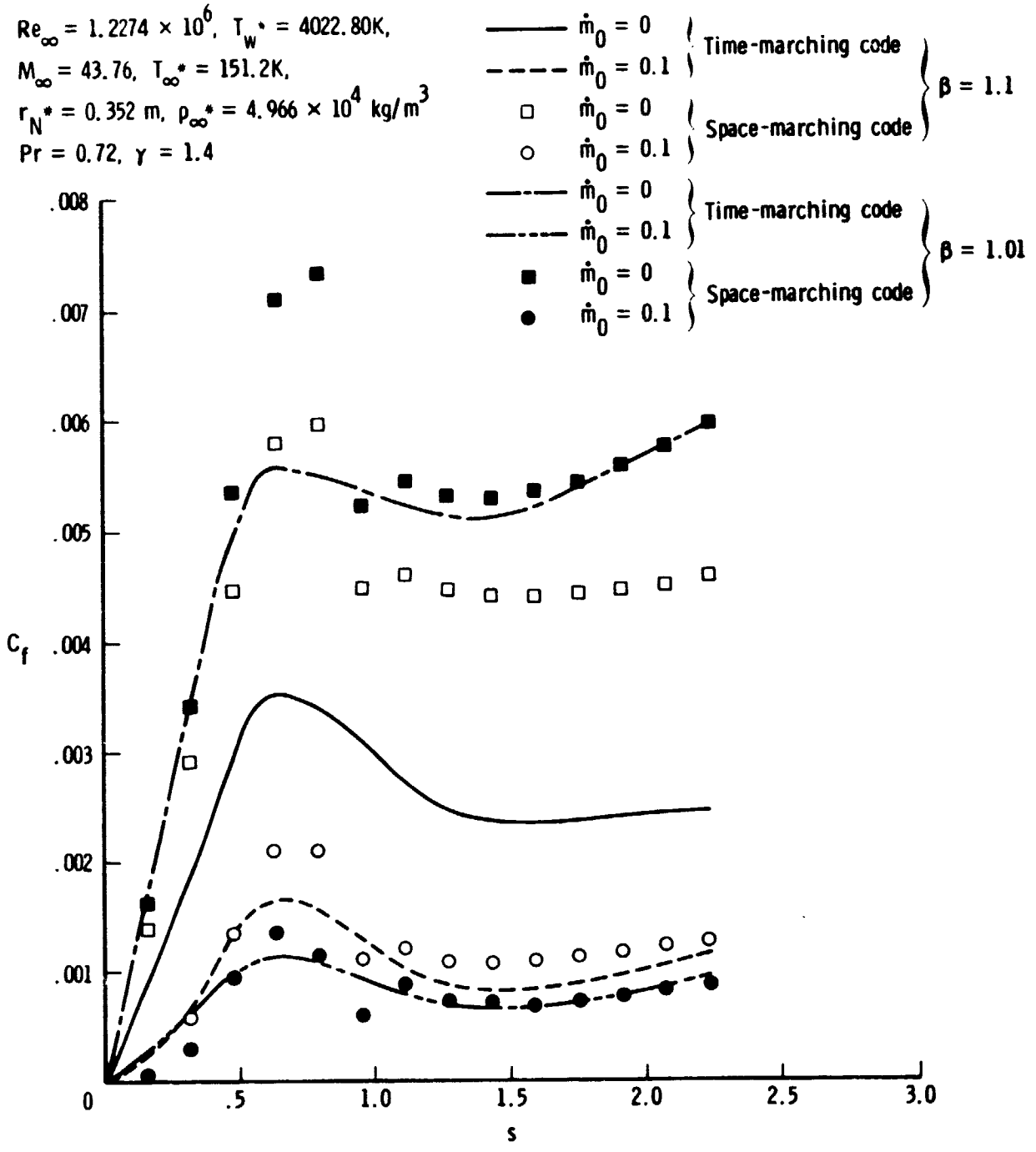

(a) Skin-friction coefficient.

Fig. 9 Comparison of wall quantities for two solution methods.

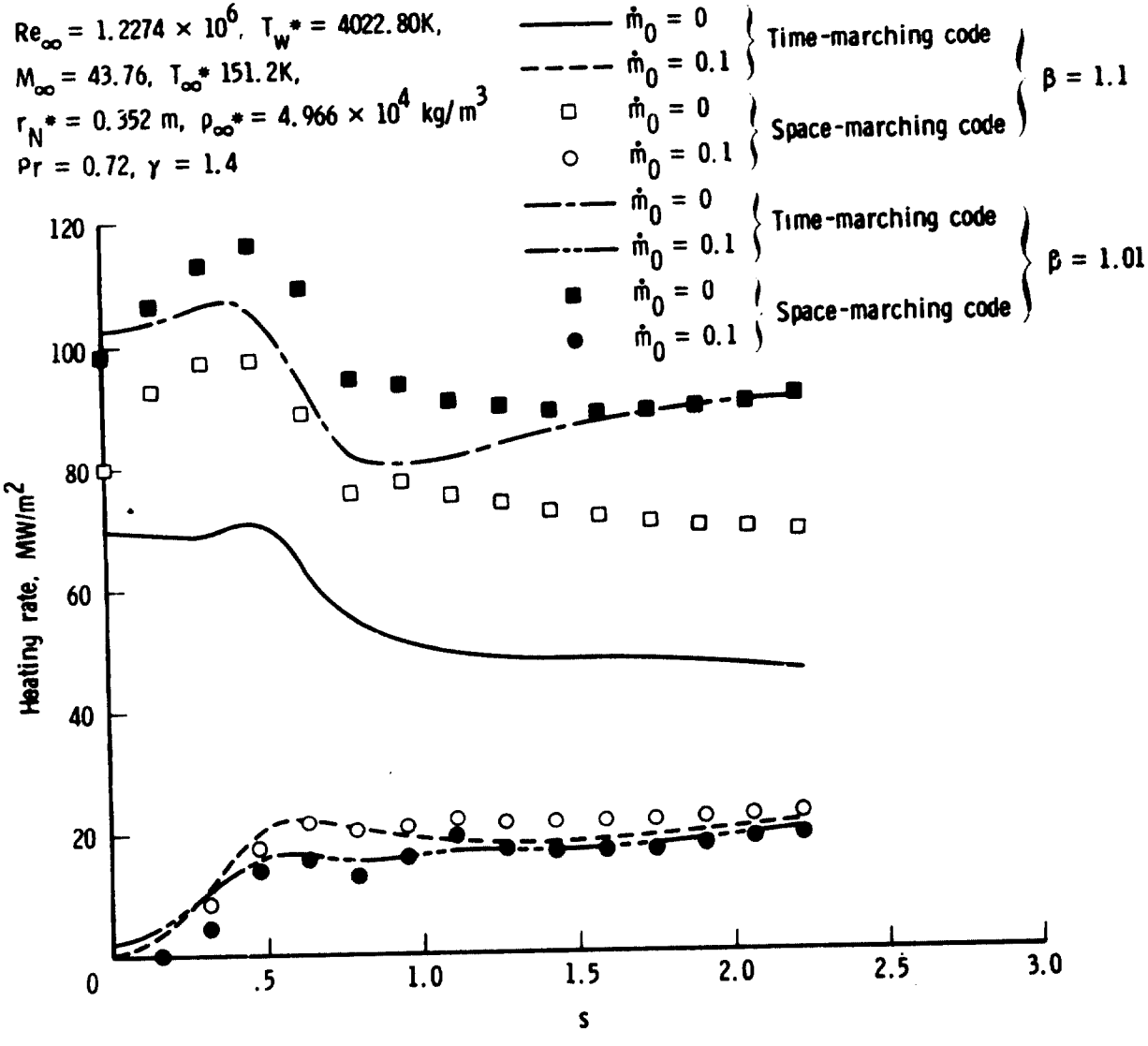

(b) Heating rate.

Fig. 9 Continued.

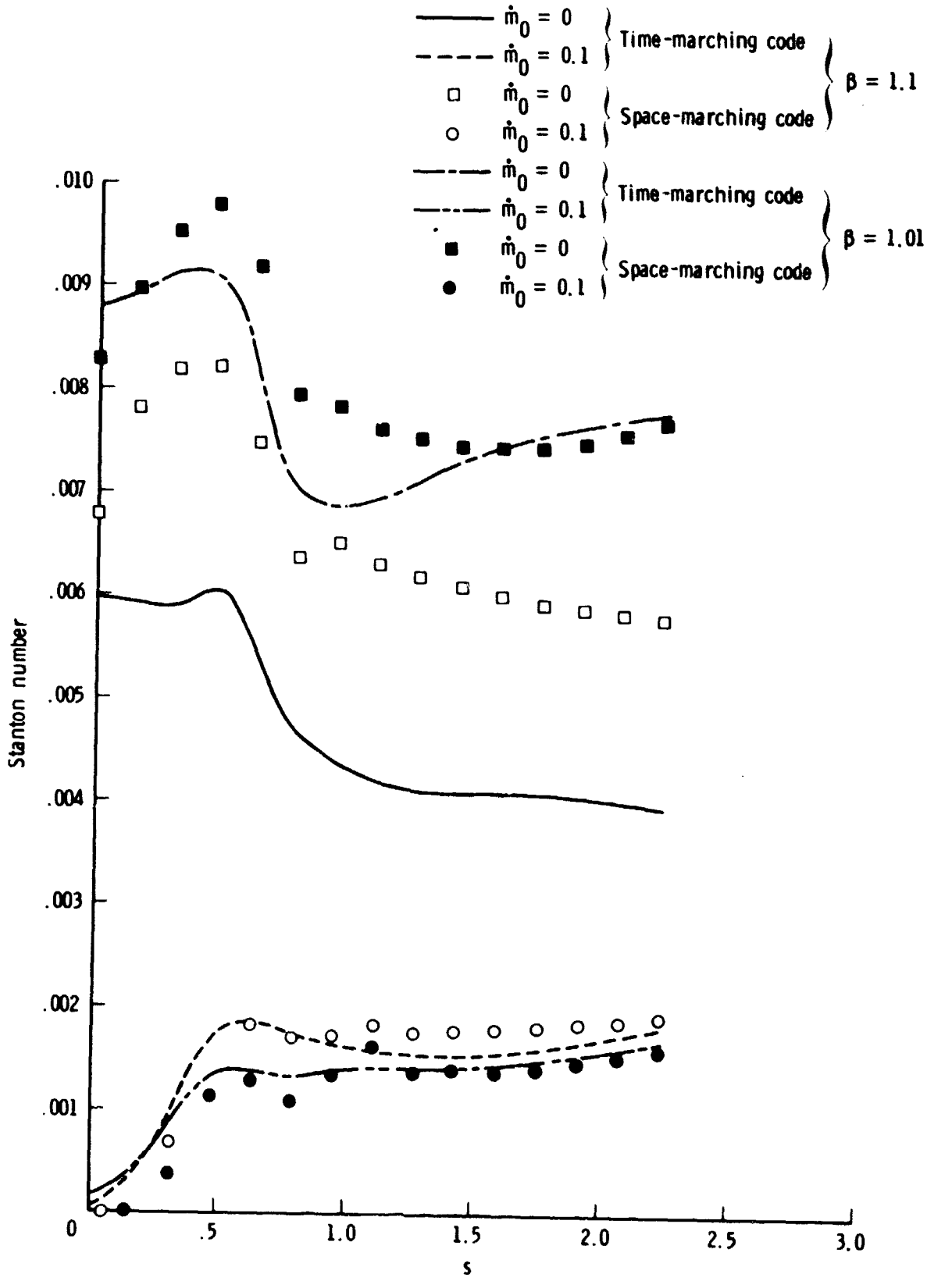

(c) Stanton number.

Fig. 9 Concluded.

PNL-4259
UC-48

DEVELOP REAL-TIME DOSIMETRY CONCEPTS AND INSTRUMENTATION FOR LONG-TERM MISSIONS

Technical Progress
February 1981 to February 1982

L.A. Braby

May 1982

Prepared for
National Aeronautics and Space Administration
Lyndon B. Johnson Space Center
Order No. T-794H
under a Related Services Agreement
with the U.S. Department of Energy
under Contract DE-AC06-76RLO 1830

Pacific Northwest Laboratory
Richland, Washington 99352

CONTENTS

FIGURES

TABLES

DEVELOP REAL-TIME DOSIMETRY CONCEPTS AND INSTRUMENTATION FOR LONG TERM MISSIONS

INTRODUCTION

Major objectives in the process of developing a rugged portable instrument to evaluate dose and dose equivalent have been achieved. A tissue-equivalent proportional counter simulating a 2 micrometer spherical tissue volume has operated satisfactorily for over a year. The basic elements of the electronic system have been designed and tested. And finally, the most suitable mathematical technique for evaluating dose equivalent with a portable instrument has been selected. Design and fabrication of a portable prototype, based on the previously tested circuits, is underway.

DETECTOR DEVELOPMENT

The 5.7 cm detector has been operated for over 15 months with the original gas filling. Figure 1 shows the gas gain for a constant anode voltage during that time. The long-term drift, less than one percent per month, and short-term (less than 24 hour) variations of ± 2 percent can easily be controlled by adjusting the anode voltage, (see Figure 2). These adjustments will be made automatically by a subroutine, illustrated in Figure 3, which compares the actual position of a calibration peak with the position of that peak at the proper gas gain. The difference is used to calculate a new high-voltage supply setting. The actual voltage is provided by a high-voltage supply referenced to the output of a digital-to-analog converter.

The detector will be operated with a combination of gas gain and electronic gain which results in a calibration factor of 0.12 keV/μm/channel and a useful range of 0.36 to 300 keV/μm. Since the dose mean of the single-event distribution for X and γ rays varies from 0.7 to 3.0 keV/μm, and for neutrons from 30 to 130 keV/μm, the system is expected to detect photon as well as neutron dose. However, the stainless steel vacuum chamber surrounding the detector will distort the response as a function of photon energy. Also, the photon-induced events cannot be distinguished from very low-energy neutron events.

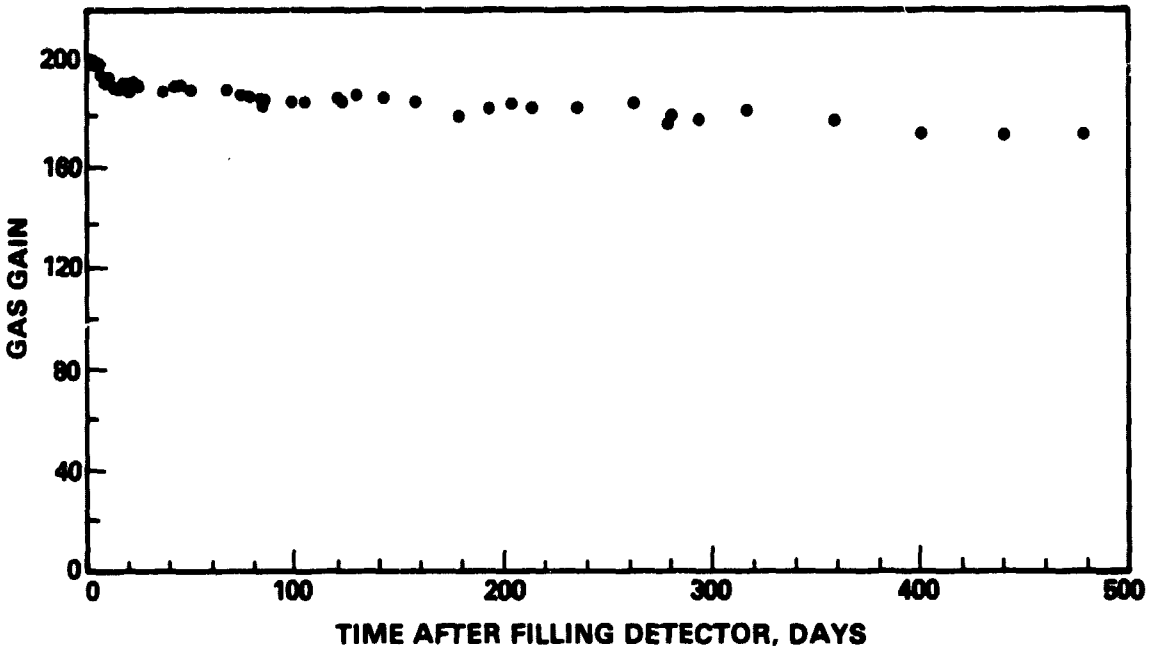

FIGURE 1. Detector Gas Gain at A Constant Anode Voltage as a Function of Time After Sealing the Detector

Thus, though the system is expected to accurately measure dose due to photons and low-energy neutrons, estimates of the mean quality factor become less certain when low-energy neutrons are abundant.

Specifications for the second detector, intended to detect high-energy heavy particles, have been completed. It will use the same basic design and materials but will be 12.7 cm in diameter in order to provide approximately five times the counting rate.

ELECTRONIC SYSTEM

The electronics for a system using two detectors is outlined in Figure 4. Each detector is supported by a dedicated high-voltage supply, amplifiers and analog-to-digital converters (ADC's), but the two detectors share a multichannel analyzer (MCA) and microcomputer. The ADC's output is used as a MCA memory address. Each event results in a "one" being added to the memory content at

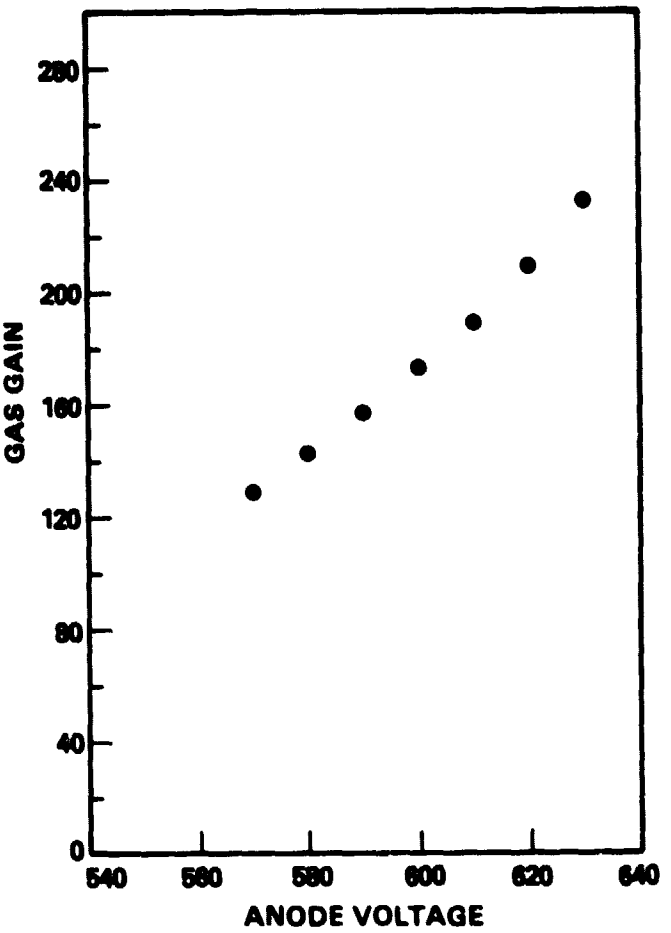

FIGURE 2. Gas Gain Versus Anode Voltage

the corresponding address. As illustrated in Figure 5, the entire MCA content can be periodically transferred to the microcomputer memory. The dosimetric quantities can then be computed without interrupting further data collection. An absolute time clock in the microcomputer is used to initiate the dose calculation, data storage, calibration and other functions. A CMOS successive approximation ADC chip and other CMOS components are used in the ADC circuit, in Figure 6, to minimize power consumption.